Research article

Robust and transparent dust removal coating applied to polyimide-based photovoltaic modules for lunar rovers

Tao Huang [a], Meihong Shen [a], Linlin Song [b], Yang Yang [b], Bin Yu [a,**], Meifang Zhu [a], Hao Yu [a,*]

[a] State Key Laboratory for Modification of Chemical Fibers and Polymer Materials, College of Materials Science and Engineering, Donghua University, Shanghai, 201620, China
[b] State Key Laboratory of Space Power Sources, Shanghai Institute of Space Power Sources, Shanghai, 200245, China

A R T I C L E   I N F O

A B S T R A C T

Dust removal coatings for polyimide (PI)-based photovoltaic modules used in lunar rovers were fabricated successfully through the blade-coating method using silicon dioxide (SiO_2) nano-particles and γ-aminopropyltriethoxysilane (KH550). The dust removal performance, morphology, transparency, and adhesive force of the coating can be optimized by adjusting the pH and the mass ratios of SiO_2 and KH550. The designed coating demonstrates excellent dust removal performance, achieving an percentage of over 85 %. Moreover, the coating has minimal impact on the transparency of the PI substrate and exhibits strong adhesion to it. Additionally, the coating shows remarkable resistance to both high and low temperatures. Even after undergoing five cycles of thermal treatment ranging from −196 to 160 °C, there were no significant changes in the morphology or dust removal performance of the coating. Therefore, this coating exhibits tremendous potential for application in the dust removal of photovoltaic modules in lunar rovers.

1. Introduction

With the advancement of lunar exploration missions both domestically and internationally, lunar dust has garnered significant attention and is recognized as a challenge that must be addressed before humans can return to the moon [1]. This is primarily due to the fact that minuscule lunar dust particles have a tendency to become charged and adhere to the surface of lunar exploration equipment, subsequently impairing the equipment's normal functionality [2,3]. As the exclusive source of energy for lunar exploration devices, flexible photovoltaic modules require robust protection against the pervasive threat of lunar dust. The deposition of this dust on the modules' surfaces can significantly impair their light transmittance, consequentially diminishing their photovoltaic efficiency [4,5]. The deposition of lunar dust caused the output of solar cells on Apollo 15 decreased by 16 % within one year [6]. According to data from the lunar dust detector on the Chang'E−3 lander, the short-circuit current loss was 16.72 % when the deposition density of lunar dust reached 0.83 mg/cm^2 [7]. Therefore, developing effective dust removal methods is an important guarantee for the efficient and stable operation of lunar rover photovoltaic systems.

So far, dust removal methods can be divided into two categories: active and passive methods. The active method involves the use of

* Corresponding author.
** Corresponding author.
E-mail addresses: yubin@dhu.edu.cn (B. Yu), yh@dhu.edu.cn (H. Yu).

external forces to prevent dust accumulation, such as air blowing [8], mechanical sweeping, and electrostatic expelling [1,9,10]. However, the gas used in air blowing cannot be recycled, leading to resource wastage. The mechanical sweeping method requires manual operation and the hard bristles may potentially damage the equipment surface. On the other hand, the electrostatic method has gained significant attention due to its simple structure and high dust removal percentage, resulting in extensive research. This method relies on the utilization of electrostatic traveling and standing waves to displace lunar dust from the surface of solar panels. Nonetheless, the electrostatic method necessitates an external high-voltage power source, and its efficacy may be compromised under vacuum conditions. Unlike the active method, the passive method seeks to reduce the adhesion between dust and the protected surface by utilizing surface modification technology. Coating the photovoltaic modules surface with a hydrophilic and hydrophobic coating proves to be more practical and feasible for the lunar rover.

The dust mitigation mechanism of hydrophilic and hydrophobic coatings is to lessen the effect of van der Waals forces, which are responsible for the adhesion between dust particles and the surface of the substrate [11–16]. The composition and roughness of the surface are crucial factors in determining the strength of van der Waals Forces [17–20]. Wang et al. [21] utilized superhydrophilic coatings on a photovoltaic glass modules using dual base/acid-catalyzed sol–gel method, which exhibited high transparency and low adhesion to dust. Zhang et al. [18] prepared a series of hydrophobic hybrid coatings on glass and demonstrated that the surface roughness is vital to dust removal property and low energy modification can further lower the adhesion force between the surface and dust. Jang et al. [22] conducted a comparative study on the anti-dust properties of superhydrophilic and superhydrophobic coatings on mirror substrates. Both types of coatings exhibited excellent anti-dust performances, which were attributed to the reduction of adhesion force due to surface roughness. However, long-term outdoor experiments revealed that the superhydrophilic coating with nanoscale roughness demonstrated relative long-term stability, making it a suitable choice for solar panel applications. Thus, the optimal surface composition and roughness of the coating are crucial factors in achieving high dust removal performance [15].

Based on the above, currently, most dust removal coatings are targeted for glass surfaces and are applied in terrestrial environments [23–31]. The fabrication of dust removal coatings on flexible photovoltaic modules for lunar rovers poses a significant challenge due to the unique lunar environment and the transparency requirements of the flexible photovoltaic system. In fact, transparent polyimide (PI) film is selected as the substrate for flexible photovoltaic modules due to its excellent thermal stability, low temperature resistance and mechanical properties. Therefore, how to construct a robust dust removal coating on the surface of the PI film is a pressing issue that has been rarely reported. In addition, the moon's high vacuum conditions cause the temperature to vary dramatically between $-180\,^{\circ}$C and $120\,^{\circ}$C during day and night alternations [32]. These thermal fluctuations present a significant challenge to dust removal coatings. Given the operational environment of flexible solar panels, besides the dust removal performance, it becomes vital to assess the transparency, flexibility, thermal shock resistance and adhesive force of the coating as essential properties in evaluating their effectiveness.

In this work, silicon dioxide (SiO_2) nanoparticles and γ-aminopropyltriethoxysilane (KH550) were used to prepare transparent dust removal coatings on PI substrate by blade-coating method. The coated PI with SiO_2-to-KH550 mass ratios of 1:1 and 1:1.5 showed high transparency and excellent dust removal property due to surface roughness. The wettability and adhesive force of the coating can be controlled by adjusting SiO_2/KH550 mass ratio. After 3000 bending tests, the transparency of the coating remains almost unchanged, indicating excellent flexibility. The thermal shocks ranging from $-196\,^{\circ}$C to $160\,^{\circ}$C do not destroy the nanoporous rough structure of the coating. Even after 5 cycles, the dust removal percentage of the coating shows almost no change. These results demonstrate the significant potential of the coating for dust removal on the surface of PI based flexible photovoltaic modules used in lunar rovers.

2. Experimental

2.1. Materials

Silicon dioxide (SiO_2) nanoparticles were purchased from Evonik Co., Ltd. (Germany). γ-aminopropyltriethoxysilane (KH550) (≥98.0 %) and hydrochloric acid (HCl) (37 %) were purchased from the Sinopharm Chemical Reagent Co., Ltd. (Shanghai, China). Ethanol (≥99.7 %) was provided from Titan Technology Co. Ltd. (Shanghai, China). Deionized water was prepared in lab. All chemicals were used as received without further purification. Transparent Polyimide (PI) substrate was supplied by Hai Rui Electronic Materials Co., Ltd. (Dongguan, China). Volcanic ash sourced from Wudalianchi volcano (Heilongjiang, China) was utilized as a simulant for lunar dust. The morphology and chemical elements of the volcanic ash were analyzed by SEM and EDS (Fig. S1). The shape is irregular and the chemical elements it contains (Si, O, Al, Ca and Mg) are included in the chemical composition of lunar dust.

2.2. Preparation of SiO_2/KH550 coating

SiO_2 nanoparticles were dispersed in ethanol and sonicated for 30 min to obtain a homogeneous SiO_2 suspension with a concentration of 1 wt%. A total of 10 g of SiO_2 suspension and varying amounts of KH550 were mixed together, following SiO_2-to-KH550 mass ratios of 1:1, 1:1.5, 1:2, and 1:2.5. Subsequently, a specific quantity of hydrochloric acid were added to adjust the pH value. The mixture was stirred at 600 rpm for 30 min at $60\,^{\circ}$C and then rapidly cooled in ice water. After an additional 30 min of sonication, the SiO_2/KH550 coating solution was ready for blade-coating. The SiO_2/KH550 coating was applied onto a cleaned PI substrate (5 cm × 8 cm) using a coating blade with a speed of 15 mm/s. The coated PI was then heated at $120\,^{\circ}$C for 1 h to remove any remaining solvent and cure the coating.
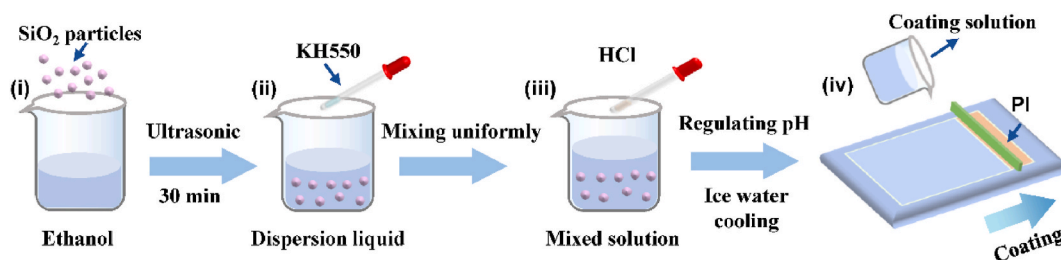
Fig. 1. The fabrication process of the SiO_2/KH550 coating.

2.3. Characterization

2.3.1. Surface morphology

S-4800 field emission scanning electron microscope (SEM, Hitachi, Japan) was performed to observe the surface morphology of the coating. The coating samples were treated with spraying gold before observation and examined under the accelerated voltage of 5 kV. The three-dimensional morphology and surface roughness (Sq, the root mean square roughness) of the coating was characterized using an Agilent 5500 atomic force microscope (AFM, Agilent, USA) in tapping mode.

2.3.2. Optical property

UV-3600 ultraviolet visible-near infrared spectrometer (Shimadzu, Japan) was used to measure the transmittance of the bare and coated PI film. Transmission spectra ranged from 300 to 1300 nm and the average transmittance was obtained by integrating the transmission spectra in this range.

2.3.3. Chemical composition

Fourier transform infrared spectrum (FTIR) was recorded using a Nicolet iS50 infrared spectrometer (Nicolet, USA) at a wavenumber of 400–4000 cm^{-1}.

2.3.4. Adhesion test

The adhesion of the coating was tested by peeling off the coatings from the PI substrate using transparent tape (3 M).

2.3.5. Wettability

Water contact angles were measured by an OCA 40 Micro contact angle-measuring instrument (DataPhysics Instruments GmbH, Germany) which used a 3 μL water droplet and measured three different positions on the coating surface each time.

2.3.6. Dust removal performance

Dust removal tests were conducted using a custom-built device consisting of a transparent acrylic box with three vents, a dust holder, and two sample holders tilted at an angle of 45°. The specific test procedures were as follows: a coated PI sample and a bare PI sample were fixed on the respective sample holder. Then, 5g of volcanic ash was placed on the dust holder, and the device cover was closed. Airflow was applied for 30 s to disperse the dust into the air, and the samples were weighed after standing for 5 min. The dust removal percentage (D_R) of the coating was calculated by:

$$D_R = \frac{W_0 - W_1}{W_0} \times 100 \tag{1}$$

Where W_0 is the dust deposition weight of the bare PI and W_1 is the dust deposition weight of the coated PI.

2.3.7. Bend-resistant performance

The bend resistant performance involved securing the coated PI to a specialized motor and folding it using the motor's reciprocating motion.

2.3.8. Thermal stability

Thermogravimetric analysis (TGA) and derivative thermogravimetric analysis (DTG) were carried out using TG 209 F1 thermogravimetry (Netzsch, Germany) under nitrogen atmosphere at a heating rate of 20 °C/min. About 6–8 mg sample was heated within the temperature range of 30–800 °C. The coating sample was also carried out by isothermal TGA that heated up to 160 °C with a nitrogen atmosphere at a heating rate of 20 °C/min and hold at 160 °C for 1 h.

2.3.9. Thermal shock resistance

The optimized coated PI sample was exposed to extreme thermal shock cycles. Firstly, it was immersed in liquid nitrogen for 10 min, followed by heating at 160 °C for 10 min under vacuum conditions. This thermal shock cycle (−196 °C–160 °C) was repeated five
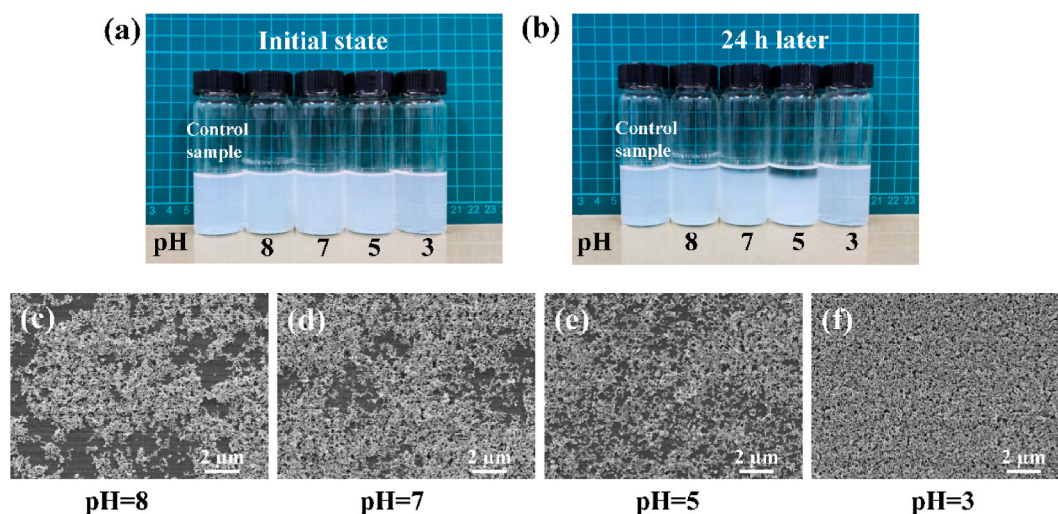
Fig. 2. The stability of bare SiO$_2$ (Control sample), SiO$_2$/KH550 coating solution and the corresponding coating morphology under different pH conditions. (a) Initial state of the coating solution; (b) Left undisturbed for 24 h; The morphology of the coatings with (c) pH = 8; (d) pH = 7; (e) pH = 5; (f) pH = 3.

times. After each thermal shock cycle, the dust removal percentage of the samples was measured, while the transmittance of the samples was measured before and after the thermal shock resistance test. The experiment utilized three parallel samples.

3. Results and discussion

3.1. The morphology of SiO$_2$/KH550 coating

The fabrication procedure of SiO$_2$/KH550 coating is shown in Fig. 1. It involves dispersing SiO$_2$ nanoparticles in ethanol through ultrasonic treatment, followed by the addition of KH550. The pH value is adjusted to promote its hydrolysis at a certain temperature. Then, the solution is cooled and aged in an ice bath to obtain the coating solution. Finally, the coating solution is evenly applied to a transparent PI substrate using an automatic coating machine, cured at 120 °C, and the dust removal coating is obtained. Particularly, influences of the pH and mass ratio of SiO$_2$/KH550 on the properties of the coatings were investigated.

Fig. 2 shows the stability of SiO$_2$/KH550 coating solution and the corresponding coating morphology under different pH conditions, when the SiO$_2$-to-KH550 mass ratio was 1:1.5. Bare SiO$_2$ dispersions without KH550 was acted as control sample. The digital photo clearly demonstrates the effect of pH on the dispersion state of the SiO$_2$/KH550 coating solution. In comparison to the control sample, the transparency of the coating solution slightly decreased at pH 8, and significantly decreased at pH 7 and 5 (Fig. 2a). However, at pH 3, the transparency was similar to that of the control sample. These findings indicate that pH strongly influences the dispersion size of SiO$_2$/KH550, which is further confirmed by the particle size test (Table S1). Additionally, when the samples were left undisturbed for 24 h, all except for pH 3 and the control sample experienced some degree of sedimentation (Fig. 2b). This suggests that the SiO$_2$/KH550 coating solution achieves excellent dispersion stability under pH 3 conditions. The morphology of the corresponding SiO$_2$/KH550 coatings with various pH values are depicted in Fig. 2c–f. It can be observed that when pH = 8, effective connections between SiO$_2$ nanoparticles were not formed, resulting in incomplete coverage of the PI substrate. Consequently, large areas of the PI surface were exposed (Fig. 2c). This is attributed to the fact that in an alkaline environment, KH550 primarily undergoes hydrolysis reactions with slow condensation, leading to inadequate crosslinking of silica. As the pH decreases, the condensation rate increases, and SiO$_2$ nanoparticles crosslink by the hydrolysis of KH550, progressively forming a denser coating (Fig. 2d and e). When the pH of the system reaches 3, SiO$_2$/KH550 effectively covers the entire PI film, resulting in a relatively complete coating (Fig. 2f). The hydrolysis and condensation reactions of KH550 under the pH of 3 are also confirmed by FTIR shown in Fig. S2. It can be observed that due to partial hydrolysis, the asymmetric stretching vibration peak and symmetric stretching vibration peak of the –CH$_3$ group in Si–O–CH$_2$CH$_3$ at 1389 cm^{-1} and 2883 cm^{-1} respectively weaken and broaden, compared with KH550. Furthermore, a new strong absorption peak at 3440 cm^{-1} indicates the formation of Si–OH bonds resulting from KH550 hydrolysis. The symmetric stretching vibration peak of Si–O–Si bonds at 877 cm^{-1} also suggests the occurrence of a condensation reaction between hydrolyzed KH550 molecules.

Furthermore, mass ratios of SiO$_2$/KH550 on the properties of the coatings under the pH of 3 were investigated. All coating solutions demonstrate excellent stability, exhibiting no observable sedimentation even after standing for 24 h (Fig. S3). Interestingly, the dispersion size of SiO$_2$ first decreases and then increases with the increase of KH550 content (Table S2). This is because, with the addition of a small amount of KH550, most of the hydroxyl groups on the surface of SiO$_2$ particles are replaced by –CH$_2$CH$_2$CH$_2$NH$_2$, preventing aggregation between adjacent SiO$_2$ particles, thus reducing the dispersion size. However, as the KH550 content continues to increase, a large amount of KH550 undergoes hydrolysis and grafts onto the surface of SiO$_2$ particles through condensation
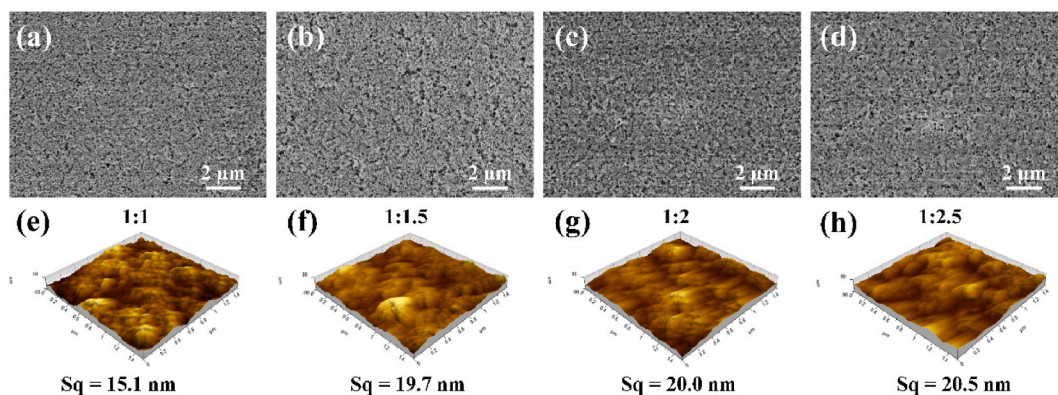
Fig. 3. SEM and AFM images of the coatings prepared with SiO_2/KH550 mass ratios of (a, e) 1:1, (b, f) 1:1.5, (c, g) 1:2, (d, h) 1:2.5.
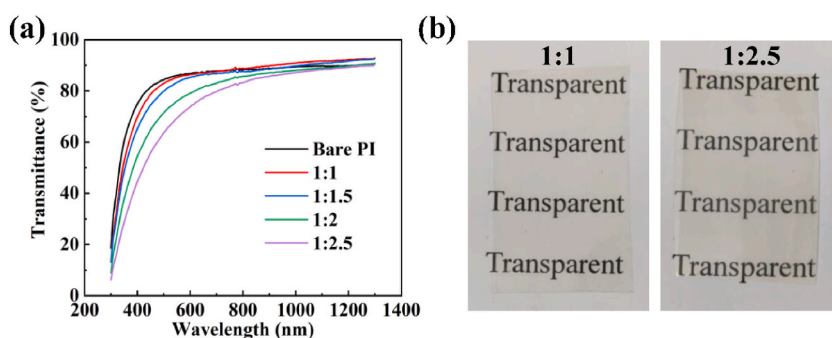

Fig. 4. (a) Transmission spectra of the bare PI and the coated PI with different SiO_2/KH550 mass ratios; (b) Digital photos of the coated PI with SiO_2/KH550 mass ratios of 1:1 and 1:2.5.
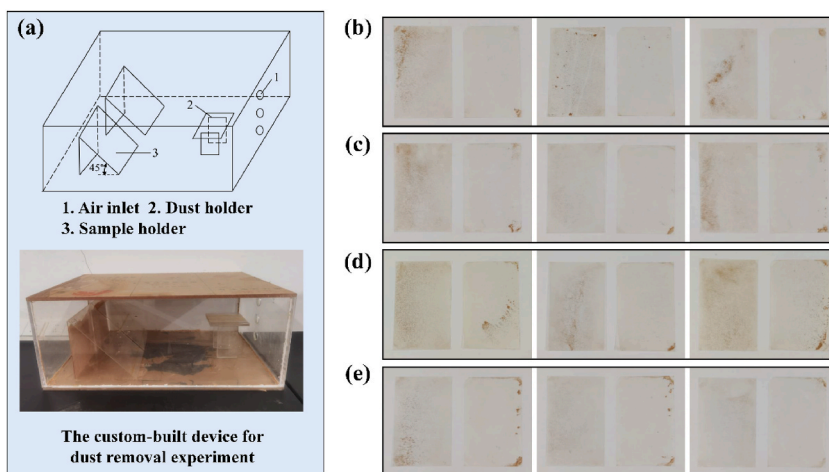

Fig. 5. The photos of the dust removal experiment. (a) The custom-built device for dust removal experiment. Photos of the dust deposited bare PI (the left side of each group of photos) and the SiO_2/KH550 coated PI (the left side of each group of photos) with mass ratio of (b) 1:1, (c) 1:1.5, (d) 1:2, (e) 1:2.5.

reactions, leading to cross-linking between SiO_2 particles through KH550 (Fig. S4), resulting in the increase of dispersion size. Fig. 3a–d displays the morphology of the SiO_2/KH550 coatings with varying KH550 content. All the samples demonstrate a similar surface morphology, indicating that the hydrolyzed KH550 cross-linked the SiO_2 nanoparticles, resulting in a compact structure. To further examine the three-dimensional morphology and surface roughness of the coatings, an AFM analysis was conducted. The AFM images in Fig. 3e–h vividly reveal that the surface of the coatings is not flat but rather rough, attributed to the presence of KH550-
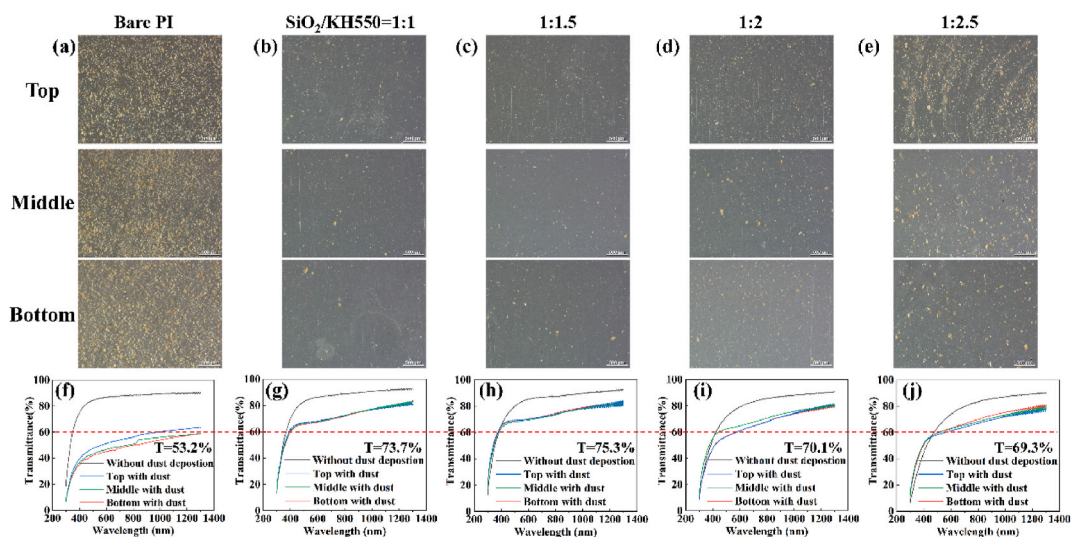
Fig. 6. The super depth-of-field microphotographs of (a) bare PI and the coated PI ((b) 1:1, (c) 1:1.5, (d) 1:2, (e) 1:2.5) with dust deposition at the top, middle, and bottom positions, respectively; The transmittance curve of (f) bare PI and coated PI ((g) 1:1, (h) 1:1.5, (i) 1:2, (j) 1:2.5) with dust deposition at the top, middle, and bottom positions, respectively.

Table 1
The detail data of the dust deposition test and the dust removal percentage of the coatings.

SiO_2/KH550 mass ratio	W_0(g)	W_1(g)	D_R(%)	
			Individual	Average
1:1	0.0136	0.0021	84.6	86.7
	0.0105	0.0009	91.4	
	0.0138	0.0022	84.1	
1:1.5	0.0177	0.0028	84.2	85.5
	0.0092	0.0008	91.3	
	0.0147	0.0028	81.0	
1:2	0.0199	0.0066	66.8	62.1
	0.0150	0.0056	62.7	
	0.0209	0.0090	56.9	
1:2.5	0.0117	0.0045	61.5	62.9
	0.0099	0.0037	62.6	
	0.0068	0.0024	64.7	

modified SiO_2 aggregates. With a decrease in the SiO_2/KH550 mass ratio from 1:1 to 1:2.5, the Sq roughness values of the coatings increased from 15.1 nm to 20.5 nm.

3.2. The optical property of SiO₂/KH550 coating

With respect to the dust removal coating applied on the solar panels of the lunar rover, it is essential to ensure not only its effectiveness in preventing dust accumulation but also the retention of high transparency. This factor is crucial as it directly influences the efficiency of power generation. Therefore, controlling the roughness is necessary to minimize the intensity of light scattering and construct transparent coatings. Fig. 4a illustrates the transmission spectra of the bare PI and the coated PI with varying SiO_2/KH550 mass ratios within the wavelength range of 300–1300 nm. The spectral shows that with the increase in the proportion of KH550, the optical transparency of the coating decreases. This may be due to an increase in roughness, which enhances light scattering [33]. When the SiO_2/KH550 mass ratios of the coating are 1:1 and 1:1.5, the transmittances of the coated PI are 87.6 % and 86.4 % respectively, which are very close to the transmittance of the bare PI (87.0 %). However, when the mass ratio is 1:2.5, the transmittance of the coated PI decreases to 80.6 %. Additionally, a decrease in transparency that is visible to the naked eye can also be observed in the digital photographs (Fig. 4b).

3.3. Dust removal performance of SiO₂/KH550 coating

The dust removal percentage of the coatings with different SiO_2/KH550 mass ratios was quantitatively measured by the custom-built device (Fig. 5a) where the bare PI was set for contrast sample. For each SiO_2/KH550 ratio, three sets of parallel experiments were
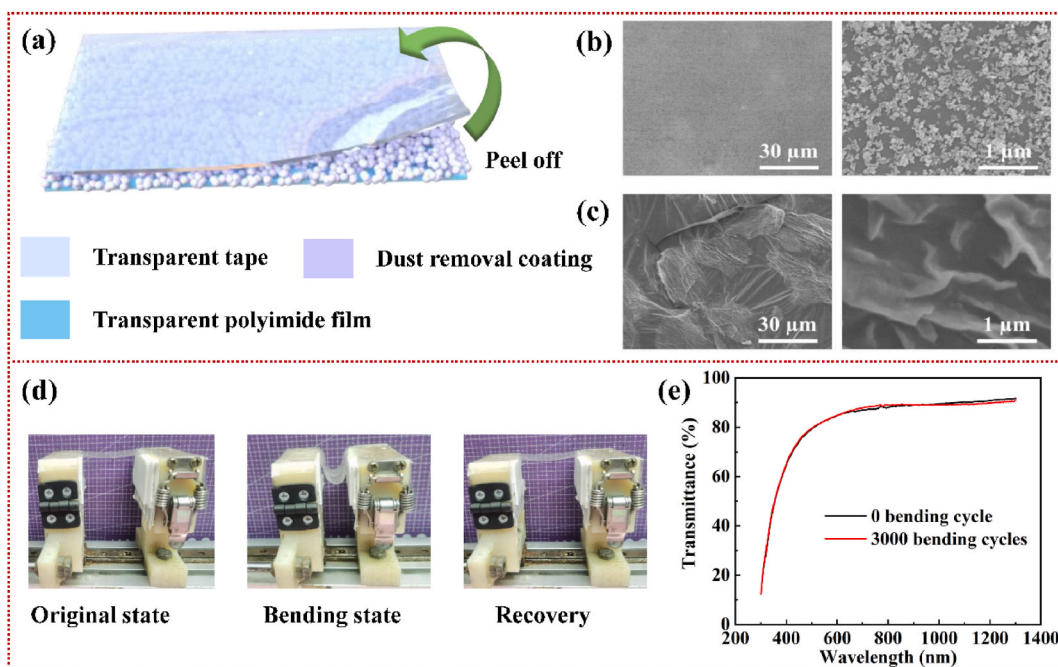
Fig. 7. Adhesion and Bend-resistant performance of SiO$_2$/KH550 coating. (a) Schematic diagram of the adhesion test; SEM images of the coating after tape adhesion. (b) SiO$_2$/KH550 = 1:1; (c) SiO$_2$/KH550 = 1:1.5; (d) Digital photos of the bending test; (e) Transmission spectra of the coated PI before and after bending for 3000 cycles.

conducted to reduce systematic errors. And the positions of the experimental and control groups were alternated once for each set of experiment. Fig. 5b–e shows the photos of the bare PI and the coated PI after the dust removal test. It can be seen that the dust deposition amount of the coated PI (right) was significantly lower than that of the bare PI (left), which indicate that the nanostructure of the SiO$_2$/KH550 can effectively reduce the contact area between dust and the coating surface and lower the adhesive force between them, thus reducing the dust deposition [19,22]. The super depth-of-field microphotographs further confirmed that the bare PI (Fig. 6a) has much more dust compared to the coated PI (Fig. 6b–e) across various positions - top, middle, and bottom. Furthermore, it was observed that when the ratio of SiO$_2$/KH550 is 1:1 and 1:1.5, the amount of dust deposition was significantly lower compared to ratios of 1:2 and 1:2.5. More importantly, the average transmittance of the bare PI film significantly decreased to 53.2 % at the top, middle, and bottom positions (Fig. 6f). In contrast, the transmittance of the PI film coated with various SiO$_2$/KH550 ratios (1:1, 1:1.5, 1:2, and 1:2.5) remained relatively higher, with average values of 73.7 %, 75.3 %, 70.1 %, and 69.3 %, respectively, at the corresponding positions (Fig. 6g–j). The above results indicate that the SiO$_2$/KH550 coating exhibits clear advantages in minimizing light transmission losses, thereby offering significant potential for ensuring stable power supply in photovoltaic systems for lunar rovers.

Table 1 presents detailed data regarding the dust deposition test and calculates the percentage of dust removal for the coatings. It can be observed that the dust removal percentage of the coating decreases with an increase in KH550 content. When the ratio of SiO$_2$/KH550 is 1:1 and 1:1.5, the coating exhibits excellent dust removal performance, with a dust removal percentage of over 85 %. However, with further increase in KH550 content, the dust removal percentage significantly decreases to around 60 %. This is because the excessive addition of KH550 provides a large number of organic groups such as –NH$_2$ and –CH$_2$CH$_3$ (This can be also confirmed by the increasing water contact angle showing in Fig. S5), thereby significantly increasing the intermolecular interaction between the coating surface and dust.

3.4. Adhesion and bend-resistant performance of SiO$_2$/KH550 coating

The adhesion and flexibility of the dust removal coating for flexible photovoltaic modules are crucial factors that determine the practical application value, alongside transparency and dust removal performance [34]. In order to evaluate these properties, tape adhesion tests were conducted on coatings with SiO$_2$/KH550 ratios of 1:1 and 1:1.5. Fig. 7a depicts the schematic diagram of the adhesion test, where the detachment of the coating from the substrate is observed after tape adhesion to determine its adhesion strength. Fig. 7b and c displays the microscopic morphology of the coating surface following tape adhesion. When the SiO$_2$/KH550 ratio is 1:1, small areas of the coating surface show detachment (Fig. 7b), thereby exposing the PI substrate. However, with a SiO$_2$/KH550 ratio of 1:1.5, the tape not only fails to peel off the coating, but instead leaves behind an adhesive layer on the surface (Fig. 7c). This observation suggests that the coating exhibits excellent bonding with the PI substrate at this particular ratio. The robust bond is a result of the cross-linking of SiO$_2$ facilitated by KH550, as well as the establishment of strong intermolecular forces such as hydrogen bonding between the amino groups of KH550 and the PI substrate.
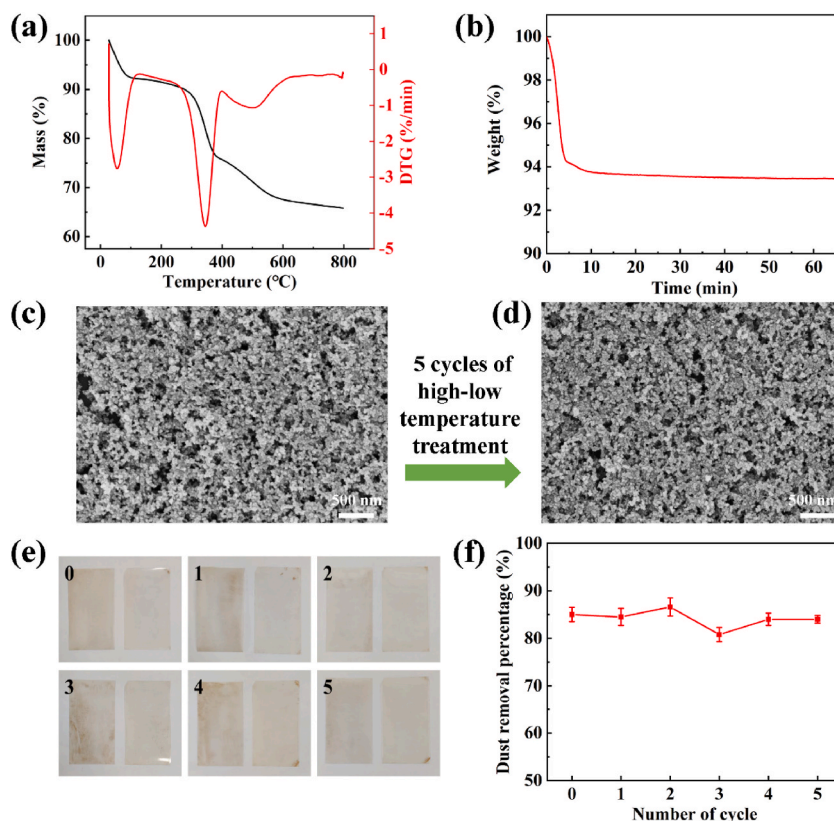
Fig. 8. Thermal shock resistance of SiO$_2$/KH550 coating. (a) Thermogravimetric and (b) isothermal thermogravimetric curve (160 °C) of the SiO$_2$/KH550 coating (1:1.5); (c) SEM image of the coating (c) before and (d) after 5 cycles of thermal shock treatment; (e) Dust removal photos of the bare PI (the left side of each group of photos) and coated PI (the right side of each group of photos) after 0–5 cycles of thermal shock treatment; (f) Dust removal percentage as a function of the number of thermal shock treatment cycles.

Considering that the PI based flexible photovoltaic modules will inevitably bend in practical applications, a bending test was conducted on a custom-designed bending stage to further investigate the adhesion strength and flexibility of the 1:1.5 coating sample (Fig. 7d). It is evident that the transmission spectra of the sample remained unchanged after 3000 bending cycles, indicating excellent resistance to bending. It is evident that after 3000 bending cycles, the sample's transmission spectra remained unchanged, indicating excellent resistance to bending (Fig. 7e).

3.5. Thermal shock resistance of SiO$_2$/KH550 coating

Due to the absence of an atmosphere on the moon, there is a substantial temperature disparity between day and night, with extreme temperatures ranging from +120 °C to −180 °C. As a result, the dust removal coating must possess exceptional resistance to both high and low temperatures. Firstly, we conducted an investigation on the thermal stability of the SiO$_2$/KH550 coating (1:1.5), as illustrated in Fig. 8a. Analysis of the TG and DTG curves revealed that the thermal decomposition process can be divided into three distinct stages. The first stage involves the vaporization of adsorbed water of the coating (<100 °C), the second stage corresponds to the dehydration condensation of silanol groups and the gradual decomposition of organic groups (>300 °C), and the third stage is identified as the rapid decomposition of organic groups (>400 °C). This indicates that the chemical composition of the coating remains essentially unchanged in environments below 300 °C, indicating its favorable thermal resistance. In addition, to assess the long-term stability of the coating under high temperature conditions on the moon, we analyzed its isothermal thermogravimetric curve at 160 °C, as illustrated in Fig. 8b. The outcomes signify a substantial initial weight loss of approximately 6 % within the first 10 min, primarily due to the evaporation of water within the coating. Subsequently, the thermogravimetric curve remains relatively steady with minimal mass loss, signifying the considerable stability of the SiO$_2$/KH550 coating at a high temperature of 160 °C.

The difference in thermal expansion coefficients between the PI film and SiO$_2$ can lead to cracking and delamination of the coating under severe thermal shocks. To investigate this, we immersed the coated PI in liquid nitrogen for 10 min, followed by transferring it to a vacuum oven at 160 °C for 10 min. This cycle was repeated five times. The surface morphology of the coating was observed, as depicted in Fig. 8c and d. It was observed that there was no significant change in the surface morphology of the coating, which can be attributed to the crosslinking of SiO$_2$ with KH550, resulting in a highly stable structure. Additionally, the dust removal performance was tested after each cycle, as shown in Fig. 8e and f. It can be observed that even after five cycles of thermal shock treatments, the dust

removal performance did not significantly decrease. Therefore, the SiO_2/KH550 coating demonstrates excellent resistance to both high and low temperatures, fulfilling the requirements for the lunar surface environment, and is expected to be a viable option for preventing dust accumulation on the surface of flexible photovoltaic components on lunar rovers.

4. Conclusions

In this paper, we prepared a transparent SiO_2/KH550 coating on the surface of a polyimide film to meet the dust removal requirements of photovoltaic modules for lunar rover. The results demonstrated that a decrease in the pH of the coating solution led to the formation of a more dense and complete coating. The crosslinking between KH550 and SiO_2, along with the strong intermolecular interaction between KH550 and the PI substrate, improved adhesion to the extent that the tape could not peel off the coating from the PI surface. However, an excessive amount of KH550 reduced the transparency of the coating and increased interaction with dust, resulting in a lower dust removal percentage. The coating exhibited the best overall performance when the pH was 3 and the SiO_2/KH550 ratio was 1:1.5, achieving a dust removal percentage of over 85 % and an average transmittance (86.4 %) comparable to that of the blank PI (87.0 %). Additionally, the coating demonstrated excellent resistance to thermal shock, maintaining stable surface morphology and dust removal percentage after 5 cycling treatments ranging from $-196°C$-160 °C. Therefore, this coating holds promise for effectively removing dust from photovoltaic modules in the lunar environment.

CRediT authorship contribution statement

Tao Huang: Writing – review & editing, Writing – original draft. **Meihong Shen:** Methodology. **Linlin Song:** Funding acquisition, Formal analysis. **Yang Yang:** Funding acquisition, Formal analysis. **Bin Yu:** Methodology, Investigation. **Meifang Zhu:** Resources, Investigation. **Hao Yu:** Supervision, Methodology, Investigation.

Declaration of competing interest

The authors declare that they have no known competing financial interests or personal relationships that could have appeared to influence the work reported in this paper.

Acknowledgement

Appendix A. Supplementary data

Supplementary data to this article can be found online at https://doi.org/10.1016/j.heliyon.2024.e31985.

References

[1] C.I. Calle, C.R. Buhler, J.L. McFall, S.J. Snyder, Particle removal by electrostatic and dielectrophoretic forces for dust control during lunar exploration missions, J. Electrost. 67 (2009) 89–92.
[2] C.I. Calle, C.R. Buhler, M.R. Johansen, M.D. Hogue, S.J. Snyder, Active dust control and mitigation technology for lunar and Martian exploration, Acta Astronaut. 69 (2011) 1082–1088.
[3] J.S. Halekas, G.T. Delory, D.A. Brain, R.P. Lin, M.O. Fillingim, C.O. Lee, et al., Extreme lunar surface charging during solar energetic particle events, Geophys. Res. Lett. 34 (2007).
[4] M. Abderrezek, M. Fathi, Experimental study of the dust effect on photovoltaic panels' energy yield, Sol. Energy 142 (2017) 308–320.
[5] Z. Wu, S.Y. Yan, T.Z. Ming, X.Y. Zhao, N. Zhang, Analysis and modeling of dust accumulation-composed spherical and cubic particles on PV module relative transmittance, Sustain. Energy Technol. Assessments 44 (2021).
[6] J.R. Bates, P.H. Fang, Results of solar-cell performance on lunar base derived from apollo missions, Sol. Energy Mater. Sol. Cells 26 (1992) 79–84.
[7] H.Y. Zhang, Y. Wang, L.P. Chen, H. Zhang, C.H. Li, J.H. Zhuang, et al., In-situ lunar dust deposition amount induced by lander landing in Chang'E-3 mission, Sci. China Technol. Sci. 63 (2020) 520–527.
[8] K. Wood, L. Belden, K. Cowan, H. Kleespies, K. Shelburne, Design of equipment for lunar dust removal, 1991. NASA.
[9] H. Kawamoto, S. Hashime, Practical performance of an electrostatic cleaning system for removal of lunar dust from optical elements utilizing electrostatic traveling wave, J. Electrost. 94 (2018) 38–43.
[10] H. Kawamoto, M. Uchiyama, B.L. Cooper, D.S. McKay, Mitigation of lunar dust on solar panels and optical elements utilizing electrostatic traveling-wave, J. Electrost. 69 (2011) 370–379.
[11] L.L. Kazmerski, A. Diniz, C.B. Maia, M.M. Viana, S.C. Costa, P.P. Brito, et al., Fundamental studies of adhesion of dust to PV module surfaces: chemical and physical relationships at the microscale, IEEE J. Photovoltaics 6 (2016) 719–729.
[12] W.P. Zhao, Y.K. Lv, Q.W. Zhou, W.P. Yan, Collision-adhesion mechanism of particles and dust deposition simulation on solar PV modules, Renew. Energy 176 (2021) 169–182.
[13] Q.F. Xu, J.N. Wang, K.D. Sanderson, Organic-inorganic composite nanocoatings with superhydrophobicity, good transparency, and thermal stability, ACS Nano 4 (2010) 2201–2209.

[14] H. Zhong, Y. Hu, Y.H. Wang, H.X. Yang, TiO2/Silane coupling agent composed two layesrs structure: a NOvel stability super-hydrophilic SElf-cleaning coating applied in PV panels, 8th International Conference on Applied Energy (ICAE2016) (2017) 1077–1083.

[15] G.A. Sobacı, O.B. Okan, K. Kazmanlı, R. Budakoğlu, Scalable deposition of sol–gel based monolayer antireflective thin films by using a dual alkoxysilane precursor chemistry, J. Sol. Gel Sci. Technol. 102 (2022) 493–503.

[16] I. Nayshevsky, Q.F. Xu, G. Barahman, A.M. Lyons, Fluoropolymer coatings for solar cover glass: anti-soiling mechanisms in the presence of dew, Sol. Energy Mater. Sol. Cell. 206 (2020).

[17] X. Wang, W.D. Wang, H. Shao, S.M. Chao, H.Y. Zhang, C.Y. Tang, et al., Lunar dust-mitigation behavior of aluminum surfaces with multiscale roughness prepared by a composite etching method, ACS Appl. Mater. Interfaces. 4 (2022) 34020–34028.

[18] J.W. Zhang, W.Q. Wang, S.X. Zhou, H.D. Yang, C. Chen, Transparent dust removal coatings for solar cell on mars and its Anti-dust mechanism, Prog. Org. Coating 134 (2019) 312–322.

[19] Y.Y. Quan, L.Z. Zhang, Experimental investigation of the anti-dust effect of transparent hydrophobic coatings applied for solar cell covering glass, Sol. Energy Mater. Sol. Cells 160 (2017) 382–389.

[20] T. Zimmermann, C. Stauch, L. Bittel, N. Jüngling, M. Muhamettursun, M. Halik, et al., Sol-gel coatings for solar cover glass: influence of surface structure on dust accumulation and removal, Sol. Energy 267 (2024).

[21] X. Wang, J.P. Nshimiyimana, D. Huang, X.G. Diao, N.N. Zhang, Durable superhydrophilic and antireflective coating for high-performance anti-dust photovoltaic systems, Appl. Nanosci. 11 (2021) 875–885.

[22] G.G. Jang, D.B. Smith, G. Polizos, L. Collins, J.K. Keum, D.F. Lee, Transparent superhydrophilic and superhydrophobic nanoparticle textured coatings: comparative study of anti-soiling performance, Nanoscale Adv. 1 (2019) 1249–1260.

[23] G. Polizos, J.K. Sharma, D.B. Smith, E. Tuncer, J. Park, D. Voylov, et al., Anti-soiling and highly transparent coatings with multi-scale features, Sol. Energy Mater. Sol. Cells 188 (2018) 255–262.

[24] L.G. Xu, J.H. He, Fabrication of highly transparent superhydrophobic coatings from hollow silica nanoparticles, Langmuir 28 (2012) 7512–7518.

[25] D. Ebert, B. Bhushan, Transparent, superhydrophobic, and wear-resistant coatings on glass and polymer substrates using SiO$_2$, ZnO, and ITO nanoparticles, Langmuir 28 (2012) 11391–11399.

[26] L.H. Jiang, P.P. Hou, S.M. He, M.M. Han, P. Xiang, T. Xiao, X.Y. Tan, The robust superhydrophobic SiO2/Diatomite/PDMS/KH-570/Me-MQ composite coating for self-cleaning application of building surface, Colloids Surf. A Physicochem. Eng. Asp. 634 (2022).

[27] H. Lu, S.W. Liang, Reduction of dust deposition on solar photovoltaic cells by self-cleaning coating: experimental study of influencing factors, Energy Technol. 9 (2021).

[28] F. Lisco, F. Bukhari, S. Uličná, K. Isbilir, K.L. Barth, A. Taylor, J.M. Walls, Degradation of hydrophobic, anti-soiling coatings for solar module cover glass, Energies 13 (2020).

[29] M.Z. Khan, G. Willers, A.A. Alowais, V. Naumann, M. Mirza, E. Grunwald, et al., Soiling mitigation potential of glass coatings and tracker routines in the desert climate of Saudi Arabia, Prog. Photovoltaics Res. Appl. 32 (2023) 45–55.

[30] M.Z. Khan, A. Abuelseoud, K. Lange, G. Willers, M.A. Bahattab, M. Mirza, et al., Correlation between laboratory and outdoor soiling experiments with anti-soiling coatings, Sol. Energy Mater. Sol. Cell. (2024) 269.

[31] M.A. Bahattab, I.A. Alhomoudi, M.I. Alhussaini, M. Mirza, J. Hegmann, W. Glaubitt, P. Löbmann, Anti-soiling surfaces for PV applications prepared by sol-gel processing: comparison of laboratory testing and outdoor exposure, Sol. Energy Mater. Sol. Cell. 157 (2016) 422–428.

[32] G.Y. Xiong, X.L. Guo, S.T. Yuan, M. Xia, Z.H. Wang, The mechanical and structural properties of lunar regolith simulant based geopolymer under extreme temperature environment on the moon through experimental and simulation methods, Construct. Build. Mater. 325 (2022).

[33] C. Wang, A.H.F. Wu, R.N. Lamb, Superhydrophobicity and optical transparency in thin films: criteria for coexistence, J. Phys. Chem. C 118 (2014) 5328–5335.

[34] X.X. Zhao, S.A. Soper, M.C. Murphy, A high-adhesion binding strategy for silica nanoparticle-based superhydrophobic coatings, Colloids Surf. A Physicochem. Eng. Asp. 625 (2021).